

Identifying Patterns Using Cross-Correlation Random Matrices Derived from Deterministic and Stochastic Differential Equations

Roberto da Silva, Sandra D. Prado

*Institute of Physics, Federal University of Rio Grande do Sul, Brazil**

Cross-Correlation random matrices have emerged as a promising indicator of phase transitions in spin systems. The core concept is that the evolution of magnetization encapsulates thermodynamic information [R. da Silva, *Int. J. Mod. Phys. C*, 2350061 (2023)], which is directly reflected in the eigenvalues of these matrices. When these evolutions are analyzed in the mean-field regime, an important question arises: Can the Langevin equation, when translated into maps, perform the same function? Some studies suggest that this method may also capture the chaotic behavior of certain systems. In this work, we propose that the spectral properties of random matrices constructed from maps derived from deterministic or stochastic differential equations can indicate the critical or chaotic behavior of such systems. For chaotic systems, we need only the evolution of iterated Hamiltonian equations, and for spin systems, the Langevin maps obtained from mean-field equations suffice, thus avoiding the need for Monte Carlo (MC) simulations or other techniques.

I. INTRODUCTION

Random matrices theory (RMT) is pivotal in deciphering the intricate behavior of quantum systems exhibiting chaotic dynamics. In the realm of quantum chaos, the statistical properties of energy levels and wavefunctions are central to understanding the underlying physics. Random matrices provide a powerful mathematical framework for modeling these properties, revealing universal patterns such as Wigner-Dyson distributions and level repulsion [1] — hallmarks of quantum chaotic systems [2, 3]. Although originating in Physics in the context of Nuclear Physics and quantum mechanics with connections with statistical physics [4, 5], random matrices theory has since found broad application across various

* Corresponding author: rdasilva@if.ufrgs.br

disciplines, including economics [6–10], neuroscience [11], and complex networks [12, 13].

In chaotic systems, characterized by extreme sensitivity to initial conditions, this theory offers a rigorous approach to analyzing the statistical properties of complex behaviors, enriching our theoretical understanding of quantum chaos and extending its relevance to fields where complexity and disorder are paramount.

Additionally, the Langevin equation and random matrices theory are intimately connected in the study of stochastic processes and complex systems in physics. The Langevin equation, a fundamental tool for modeling the dynamics of particles in fluctuating environments, describes the evolution of systems under random forces. This stochastic differential equation captures the interplay between deterministic and stochastic components, making it a cornerstone in nonequilibrium statistical mechanics [14, 15].

When applied to the Langevin equation, random matrices theory provides deep insights into the spectral properties of associated stochastic operators and the distribution of eigenvalues (see for example [16]). This connection is particularly significant for understanding disordered systems and the dynamics of large ensembles of interacting particles. By linking these two powerful frameworks, researchers can explore universal statistical patterns in complex systems, deepening our understanding of both classical and quantum phenomena.

Systems with a discrete time variable are referred to as maps. Maps describe the time evolution of significant quantities in physics, crucial for analyzing the stability, criticality, and chaotic behavior of systems [17]. For instance, given a Hamiltonian $\mathcal{H}(q, p, t)$, the evolution of generalized positions and momenta is governed by Hamilton's equations [18]:

$$\frac{dq}{dt} = \frac{\partial \mathcal{H}}{\partial p} \quad \text{and} \quad \frac{dp}{dt} = -\frac{\partial \mathcal{H}}{\partial q} \quad (1)$$

The discretization of these differential equations results in deterministic maps, which are generally expressed as:

$$p_{n+1} = p_n + g_1(q_n) \quad (2)$$

$$q_{n+1} = q_n + g_2(p_{n+1})$$

where $n = 0, 1, 2, \dots$ parametrizes time, and g_1 and g_2 are functions specific to the problem under consideration.

Similarly, in the case of a spin system in the mean-field regime, the time evolution of magnetization m is generally described by the Langevin equation [14, 19]:

$$\frac{dm}{dt} = -c \frac{\delta F(m; K_1, K_2, \dots, K_l)}{\delta m} + \Gamma \xi(t) \quad (3)$$

where $F(m; K_1, K_2, \dots, K_l)$ is the free energy of the system, and K_1, K_2, \dots, K_l are the system's parameters, which can include temperature, field, and combinations of such quantities. Here, N represents the system size, i.e., the number of spins, such that

$$\Gamma \sim \frac{1}{\sqrt{N}} \quad (4)$$

which must vanish in the thermodynamic limit, i.e., $N \rightarrow \infty$, while $\xi(t)$ represents white noise. Therefore:

$$\langle \xi(t) \rangle = 0 \quad (5)$$

$$\langle \xi(t) \xi(t') \rangle = \delta(t - t').$$

For simplicity, we denote $\varphi(m|K_1, K_2, \dots, K_l) = \frac{\delta F(m, K_1, K_2, \dots, K_l)}{\delta m}$. Using this, a map can be defined for the time evolution of magnetization:

$$m_{n+1} = m_n - \varepsilon c \varphi(m_n|K_1, K_2, \dots, K_l) + \varepsilon \Gamma \xi_n, \quad (6)$$

where ε is a parameter arising from the time discretization of the differential equation.

Thus, although both maps 2 and 6 originate the dynamics of physical systems, they embody different physical phenomena. However, the spectral properties of the cross-correlation random matrices built from their time evolution can reveal their underlying dynamics.

Considering the problem in the context of Monte Carlo (MC) simulations of the Ising, Potts models [20–22], we have shown that cross-correlation random matrices (CCRM), even with few time evolutions of the magnetization in these spin systems and using Metropolis or Glauber dynamics with a small number of MC steps, can accurately capture the criticality of the model. Our conclusion was that the density of eigenvalues exhibits gaps that govern the transition, which is reflected in the first and second moments of this density.

It is noteworthy that several authors have explored the spectral properties of CCRM in spin systems using different approaches from ours. For example, Vinayak et al. [23]

investigated the spectral properties of correlation matrices during near-equilibrium phase transitions. They studied the correlation matrices of N spins in the two-dimensional Ising model across several MC steps, revealing evidence of power-law spatial correlations at phase transitions. Similarly, Biswas et al. [24] analyzed the steady-state correlation matrix in the asymmetric simple exclusion process. It is important to note that dealing with matrices of this size, proportional to the number of spins, is computationally demanding. Our method, however, offers a significant advantage by operating with much smaller matrices, as we will demonstrate.

Alternatively, maps from Hamiltonian systems can also be used to build CCRM of one-parameter systems. In this direction, we showed that this method is able to explore the chaoticity and nuances of the logistic map and the Chirikov standard map by studying the spectra of these matrices [25].

In this current work, we take a step further. We propose to study the spectral properties of CCRM from spin systems, not through MC simulations, but by considering the proper Langevin equation describing their processes. Specifically, we use the Ising model and its spin-1 version, the Blume-Capel (BC) model. This approach is particularly interesting because it elevates the method to the level of stochastic differential equations, rather than relying on MC simulations.

Conversely, to corroborate that the properties of maps of different physical systems can be translated by the spectra of random matrices, we studied the Kicked Harper Map (KHM), a two-dimensional area preserving map that exhibits mixed dynamics [26]. This map is the classical counterpart of the quantum dynamical system known as the kicked-Harper model.

The work is organized as follows: In the next section, we explain how the method is applied to the various systems discussed in this study. We then present the results in Section III, followed by summaries and conclusions in the final section.

II. CROSS-CORRELATION MATRICES OF MAPS DERIVED FROM DETERMINISTIC AND STOCHASTIC DIFFERENTIAL EQUATIONS

Here, we define a cross-correlation matrix \mathcal{C} by using time series iterations of a given observable O that can be a generalized moment p , generalized position q , magnetization per particle m , and so on. This term, in the context of RMT, to the best of our knowledge,

originated in Econophysics [6–10] could also be referred to as a covariance matrix or a correlation coefficient matrix.

The elements of this matrix for a general observable O can be defined as follows:

$$\mathcal{C}_{ij} = \frac{\langle O^{(i)} O^{(j)} \rangle - \langle O^{(i)} \rangle \langle O^{(j)} \rangle}{\sigma_{O^{(i)}} \sigma_{O^{(j)}}}$$

which are calculated by sampling two time evolutions of length N_{steps} : $O_0^{(i)}, O_1^{(i)}, \dots, O_{n_{steps}-1}^{(i)}$ and $O_0^{(j)}, O_1^{(j)}, \dots, O_{n_{steps}-1}^{(j)}$, such that:

$$\langle O^{(k)} \rangle = \frac{1}{N_{steps}} \sum_{p=0}^{N_{steps}-1} O_p^{(k)}, \quad \langle O^{(i)} O^{(j)} \rangle = \frac{1}{N_{steps}} \sum_{p=0}^{N_{steps}-1} \sum_{q=0}^{N_{steps}-1} O_p^{(i)} O_q^{(j)}$$

with $\sigma_{O^{(k)}} = \frac{1}{(N_{steps}-1)} \sum_{p=0}^{N_{steps}-1} (O_p^{(k)} - \langle O^{(k)} \rangle)^2 \approx \langle O^{(k)2} \rangle - \langle O^{(k)} \rangle^2$.

It is important to note that the matrix \mathcal{C} , of dimension N_{sample} , can be obtained from the standardized time-evolution matrix \mathcal{M} :

$$\mathcal{M} = \begin{pmatrix} \frac{O_0^{(1)} - \langle O^{(1)} \rangle}{\sigma_{O^{(1)}}} & \frac{O_0^{(2)} - \langle O^{(2)} \rangle}{\sigma_{O^{(2)}}} & \dots & \frac{O_0^{(N_{sample})} - \langle O^{(N_{sample})} \rangle}{\sigma_{O^{(N_{sample})}}} \\ \frac{O_1^{(1)} - \langle O^{(1)} \rangle}{\sigma_{O^{(1)}}} & \frac{O_1^{(2)} - \langle O^{(2)} \rangle}{\sigma_{O^{(2)}}} & & \frac{O_1^{(N_{sample})} - \langle O^{(N_{sample})} \rangle}{\sigma_{O^{(N_{sample})}}} \\ \vdots & \vdots & & \vdots \\ \frac{O_{N_{steps}-1}^{(1)} - \langle O^{(1)} \rangle}{\sigma_{O^{(1)}}} & \frac{O_{N_{steps}-1}^{(2)} - \langle O^{(2)} \rangle}{\sigma_{O^{(2)}}} & & \frac{O_{N_{steps}-1}^{(N_{sample})} - \langle O^{(N_{sample})} \rangle}{\sigma_{O^{(N_{sample})}}} \end{pmatrix} \quad (7)$$

This allows us to verify that:

$$\mathcal{C} = \frac{1}{N_{steps}} \mathcal{M}^t \mathcal{M}. \quad (8)$$

It is known that if $O_0^{(i)}, O_1^{(i)}, \dots, O_{n_{steps}-1}^{(i)}$ are a set of independent random variables, we are in the context of the real Wishart ensemble [27–30]. In that case, the joint probability distribution of the eigenvalues is expected to be given by:

$$P(\lambda_1, \dots, \lambda_{N_{sample}}) = Z^{-1} e^{-\mathcal{H}(\lambda_1, \dots, \lambda_{N_{sample}})}, \quad (9)$$

where $Z = \int \dots \int d\lambda_1 \dots d\lambda_{N_{sample}} e^{-\mathcal{H}(\lambda_1, \dots, \lambda_{N_{sample}})}$, and

$$\mathcal{H}(\lambda_1, \dots, \lambda_{N_{sample}}) = \mathcal{H}_{auto}(\lambda_1, \dots, \lambda_{N_{sample}}) + \mathcal{H}_{int}(\lambda_1, \dots, \lambda_{N_{sample}})$$

corresponds to a Hamiltonian of a Coulomb gas with logarithmic repulsion

$$\mathcal{H}_{int}(\lambda_1, \dots, \lambda_{N_{sample}}) = - \sum_{i < j} \ln |\lambda_i - \lambda_j|, \quad (10)$$

and the term

$$\mathcal{H}_{auto}(\lambda_1, \dots, \lambda_{N_{sample}}) = \frac{N_{steps}}{2} \sum_{i=1}^{N_{sample}} \lambda_i - \frac{(N_{steps} - N_{sample} - 1)}{2} \sum_{i=1}^{N_{sample}} \ln \lambda_i \quad (11)$$

attracting the particles to the origin, with $\lambda_1, \dots, \lambda_{N_{sample}} \geq 0$. Since $N_{steps} > N_{sample}$, we have $\lambda > \frac{(N_{steps} - N_{sample} - 1)}{N_{steps}} \ln \lambda$.

In the case of potentials described by Eqs. 10 and 11, the density of states defined by:

$$\rho(\lambda) = \int_0^\infty \int_0^\infty \dots \int_0^\infty P(\lambda, \lambda_2, \dots, \lambda_{N_{sample}}) d\lambda_2 d\lambda_3 \dots d\lambda_{N_{sample}} \quad (12)$$

follows the well-known Marchenko-Pastur law [31, 32]:

$$\rho_M(\lambda) = \begin{cases} \frac{N_{MC}}{2\pi N_{sample}} \frac{\sqrt{(\lambda - \lambda_-)(\lambda_+ - \lambda)}}{\lambda} & \text{if } \lambda_- \leq \lambda \leq \lambda_+ \\ 0 & \text{otherwise,} \end{cases} \quad (13)$$

where $\lambda_{\pm} = 1 + \frac{N_{sample}}{N_{MC}} \pm 2\sqrt{\frac{N_{sample}}{N_{MC}}}$.

As previously discussed, our observable O can represent magnetization in spin systems, or simply a moment or position in dynamical systems. An interesting quantity to monitor, which describes how the density of states deviates from the non-correlated situation given by $\rho_M(\lambda)$ in Eq. 13, is the first moment of $\rho(\lambda)$, i.e., $E[\lambda] = \int_0^\infty \lambda \rho(\lambda) d\lambda$. Its estimator is obtained using the numerical density of states:

$$\langle \lambda \rangle = \frac{\sum_{i=1}^{N_{int}} \rho_N(\lambda_i) \lambda_i}{\sum_{i=1}^{N_{int}} \rho_N(\lambda_i)}, \quad (14)$$

where N_{int} is the number of bins used to calculate the numerical density of states $\rho_N(\lambda_i)$, which may differ from the expression in Eq. 13. In other words, the function $\mathcal{H}_{auto}(\lambda_1, \dots, \lambda_{N_{sample}})$ in Eq. 13 changes, leading to gaps in the density of states that are reflected in $\langle \lambda \rangle$ or higher moments $\rho(\lambda)$. Our previous work has shown that extreme values of $\langle \lambda \rangle$ are associated with phase transition critical points in spin systems [20–22] and chaotic-to-stability transitions in chaotic maps [25].

In this paper, we demonstrate that such transitions are intrinsically present in the stochastic differential equations (specifically Langevin equations) governing the dynamics of spin systems. We tested this using maps from the Ising and Blume-Capel (BC) models.

As a second contribution, we show that this method can be extended to a chaotic two-parameter dynamical system, the Kicked Harper model. In the next section, we provide an overview of these systems and explain how the \mathcal{C} -matrices are applied using the Random Matrices Theory (RMT) method described earlier.

A. Maps Derived from Langevin Equations: Ising and BC Models

In this case, we focus on Ising-like Hamiltonians, which can be generalized as follows:

$$\mathcal{H} = -J \sum_{\langle i,j \rangle} \sigma_i \sigma_j + D \sum_{i=1}^N \sigma_i^2 - H \sum_{i=1}^N \sigma_j. \quad (15)$$

If $D = 0$ and $\sigma_j = \pm 1$ (spin $1/2$), we have the standard Ising model. For $D \geq 0$ (anisotropy term) and $\sigma_j = 0, \pm 1$ (spin 1), we have the Blume-Capel model. Here, H is the external field that couples with each spin, and $\langle i, j \rangle$ denotes that the sum is taken only over the nearest neighbors in a d -dimensional lattice.

A mean-field approximation assumes that i -th spin σ_i interacts with a magnetic "cloud" represented by the average magnetization $\xi_i = \frac{1}{N} \sum_{j=1, j \neq i}^N \sigma_j$. Each spin, within its original lattice, is linked to $z = 2^d$ neighbors. The number of links in the lattice is $Nz/2$, as each spin is counted with $z/2$ links to avoid double-counting. Thus, in this approximation, the interaction term $H_{int} = -J \sum_{\langle i,j \rangle} \sigma_i \sigma_j$ must be replaced in the mean-field approximation by:

$$\mathcal{H}_{int}^{(MF)} = -\frac{Jz}{2} \sum_{i=1}^N \sigma_i \xi_i \approx -\frac{Jz}{2N} \sum_{i=1}^N \sum_{j=1}^N \sigma_i \sigma_j \quad (16)$$

Finally, the mean-field Hamiltonian can be written as:

$$\mathcal{H}^{(MF)} = -\frac{Jz}{2N} M^2 - HM + D \sum_{i=1}^N \sigma_i^2, \quad (17)$$

where $M = \sum_{i=1}^N \sigma_i$ is the magnetization of the system. For our purposes, we set $H = 0$ from this point onward.

Focusing initially on the Ising model ($D = 0$), the free energy of the system is given by:

$$f_I(m; K) = \frac{m^2}{2} - \frac{1}{K} \ln [2 \cosh(Km)], \quad (18)$$

where $K = \beta Jz$, with $\beta = \frac{1}{k_B T}$ and z as the coordination number. Thus, we can write the map for this case. Considering the equation 6 for this situation, we have:

$$m_{n+1} = (1 - \varepsilon)m_n + \varepsilon \tanh(Km_n) + \varepsilon \Gamma \xi_n \quad (19)$$

On the other hand, for the BC model, there are two parameters: $K_1 = \beta Jz$ and $K_2 = \beta D$. Consequently, the free energy is:

$$f_{BC}(m; K_1, K_2) = \frac{m^2}{2} - \frac{1}{K_1} \ln(2e^{-K_2} \cosh(K_1 m) + 1) \quad (20)$$

The map in this case is somewhat more complicated:

$$m_{n+1} = (1 - \varepsilon)m_n + \frac{2\varepsilon e^{-K_2} \sinh(K_1 m_n)}{2e^{-K_2} \cosh(K_1 m_n) + 1} + \varepsilon \Gamma \xi_n. \quad (21)$$

B. Map for a Two-Parameter Deterministic System: The Kicked-Harper Model

Chaotic behavior is fundamental in contemporary physics [17], as the understanding of non-deterministic phenomena under varying initial conditions is pivotal in numerous contexts. This includes the stabilization of seemingly simple mechanical systems, such as the inverted pendulum [33, 34], and investigations into the degenerate route to chaos in dissipative systems [35].

The identification of chaos in specific Hamiltonian systems can be accomplished using traditional methods; however, there is room for the development of various alternatives. In contrast, the theory of random matrices has provided a robust and potent toolkit for describing several aspects of physical phenomena.

Area-preserving maps play an important role in diverse fields as they are widely used for modeling complex systems. Maps of regular dynamics usually present stable islands and chaotic behavior separately or together in the phase space depending on the control parameter.

In this context, an interesting model is that of hamiltonian :

$$\mathcal{H}(q, p, t) = L \cos p + K \cos q \sum_{n=-\infty}^{\infty} \delta(t - n) \quad (22)$$

corresponding to the pulsed version of Harper's Hamiltonian:

$$\frac{dq}{dt} = \frac{\partial \mathcal{H}}{\partial p} = -L \sin p \quad (23)$$

$$\frac{dp}{dt} = -\frac{\partial \mathcal{H}}{\partial q} = K \sin q \sum_{n=-\infty}^{\infty} \delta(t - n)$$

Hence, the Kicked Harper map, which preserves the area in the phase space of the two canonical dynamical variables q and p , is defined as follows:

$$\begin{aligned} p_{n+1} &= p_n + K \sin q_n \\ q_{n+1} &= q_n - L \sin p_{n+1} \end{aligned} \quad (24)$$

The dynamics can be visualized on a torus by taking $q \bmod 2\pi$ and $p \bmod 2\pi$. Thus, the idea is to construct \mathcal{C} using the time evolutions of p and q as described by Eq. 24, and to investigate the resulting structures with our RMT method.

III. RESULTS

We have separated our results into two parts. The first part is dedicated to the study of maps derived from stochastic Langevin equations, which describe the criticality of mean-field Ising and Blume-Capel models. In the second part, we explore the applicability of our method in describing a map from a deterministic system, specifically the two-parameter Kicked Harper model.

A. Criticality of Spin Systems via the Langevin Equation

We initially conducted iterations of the Ising map (Eq. 19), mirroring the approach employed in our previous study using MC simulations [20]. To achieve this, we consider a time step of size $\varepsilon = 10^{-4}$. In this case, we obtained our observable represented by matrix elements $m_i^{(j)}$. Here, $i = 0, \dots, N_{steps} - 1$, where we used $N_{steps} = 300$ iteration steps, and j ranges from 1 to $N_{sample} = 100$ different series.

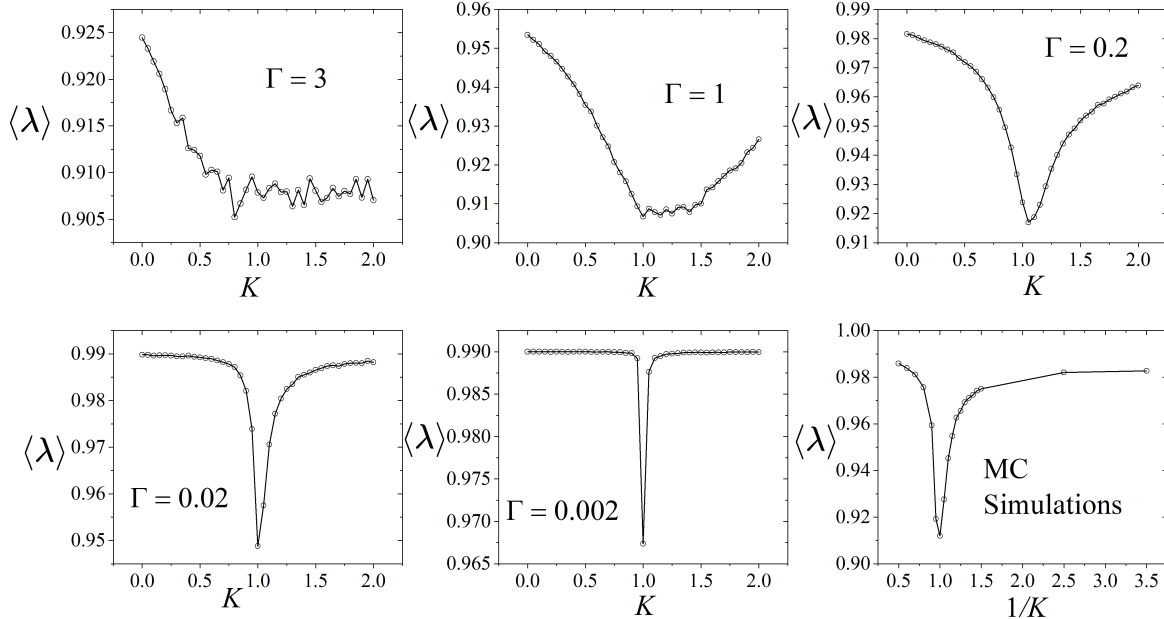


Figure 1. The average eigenvalue of \mathcal{C} as function of K for different values of Γ is shown for the mean-field Ising map. The expected transition at $K = 1$ is observed in the thermodynamic limit ($\Gamma \rightarrow 0$) and is corroborated by the method with MC simulations of magnetization evolutions. The line connecting the points is not a fit; it is provided solely for reference.

To obtain the histograms $\rho_N(\lambda) \times \lambda$, we used a total of $N_{run} = 1000$ different matrices. For all histograms we considered $N_{bin} = 100$ bins. This parameter set will also be used in all other results explored in this paper. We chose $m_0^{(j)} \in [-1, 1]$ randomly.

An important numerical point, also reported in some of our previous works, is related to constructing $\rho_N(\lambda)$ and calculating the average according to equation 14, rather than simply estimating it as an arithmetic average: $\bar{\lambda} = N_{sample}^{-1} N_{run}^{-1} \sum_{i=1}^{N_{sample}} \sum_{j=1}^{N_{run}} \lambda_{ij}$. This approach is crucial due to the sensitivity of the numerical results explored here.

Thus, we construct the ensemble of matrices \mathcal{C} for the Ising model, where the observables are captured by Eq. 19 according to Eq. 8. The results for $\langle \lambda \rangle$ as a function of K are presented in Fig. 1 for different values of Γ .

We observe that for small systems (large Γ), the average eigenvalue does not accurately reflect the expected critical value of the model ($K = 1$). However, as $\Gamma \rightarrow 0$ ($N \rightarrow \infty$), a minimum value at $K = 1$ is gradually approached. The final plot demonstrates that this

minimum value is confirmed by using time evolutions of magnetization from MC simulations of the mean-field Ising model under the Metropolis prescription (as shown in the last plot of Fig. 1 with data extracted from [22]).

It is important to note that we expect $\rho(\lambda)$ to approach $\rho_M(\lambda)$ (Eq. 13) as $K \rightarrow 0$ ($T \rightarrow \infty$), which corresponds to the paramagnetic phase. In this situation, the k -th moment, $\langle \lambda^k \rangle_{\text{numerical}}$, should closely align with the theoretical value:

$$\langle \lambda^k \rangle_{\text{exact}} = \int_{-\infty}^{\infty} \lambda^k \rho_M(\lambda) d\lambda = \sum_{j=0}^{k-1} \frac{\left(\frac{N_{\text{sample}}}{N_{\text{MC}}}\right)^j}{j+1} \binom{k}{j} \binom{k-1}{j}. \quad (25)$$

where this relation is derived by expanding the binomials and applying the well-known Vandermonde identity: $\sum_{l=0}^r \binom{m}{l} \binom{n}{r-l} = \binom{m+n}{r}$.

For $k = 1$ (which is our focus), we expect $\langle \lambda \rangle \approx 1$, as observed for $T \rightarrow \infty$ in Fig. 1. It is noteworthy that in these plots, $\langle \lambda \rangle \approx 0.99$. This small discrepancy is due to the fact that we are analyzing the evolution of magnetization rather than a single spin, leading to some spurious correlations. The fact that $\langle \lambda \rangle \approx 1$ also for $T < T_C$ is not related to $\rho(\lambda)$ approaching $\rho_M(\lambda)$; rather, it is a coincidence or an idiosyncrasy of the method, as $\langle \lambda \rangle \approx 1$ is a sufficient but not necessary condition. In fact, $\rho(\lambda)$ differs significantly from $\rho_M(\lambda)$, as observed in [20].

Thus, we can see that the method performs well at the differential equation level for the Ising model, which motivates us to apply this methodology to models with more complex phase diagrams, such as the Blume-Capel model.

The second-order phase transition line of the Blume-Capel (BC) model, in mean-field approximation, is described by the equation:

$$K_1 = 1 + \frac{e^{K_2}}{2}. \quad (26)$$

This curve ends at $(K_1, K_2) = (3, \ln 4)$, which corresponds to the tricritical point; beyond this point, the transition becomes first-order. Thus, we iterate the equation 21 by fixing K_2 and varying K_1 , while also observing the average eigenvalue, as shown in Fig. 2. Similarly, $m_0^{(j)}$ is randomly chosen from the interval $[-1, 1]$ and we also consider a time step of size $\varepsilon = 10^{-4}$.

Each plot considers systems of different sizes, and we observe that $K_1^{(C)}$ approaches the expected value as $N \rightarrow \infty$ ($\Gamma \rightarrow 0$). This is summarized in Fig. 3.

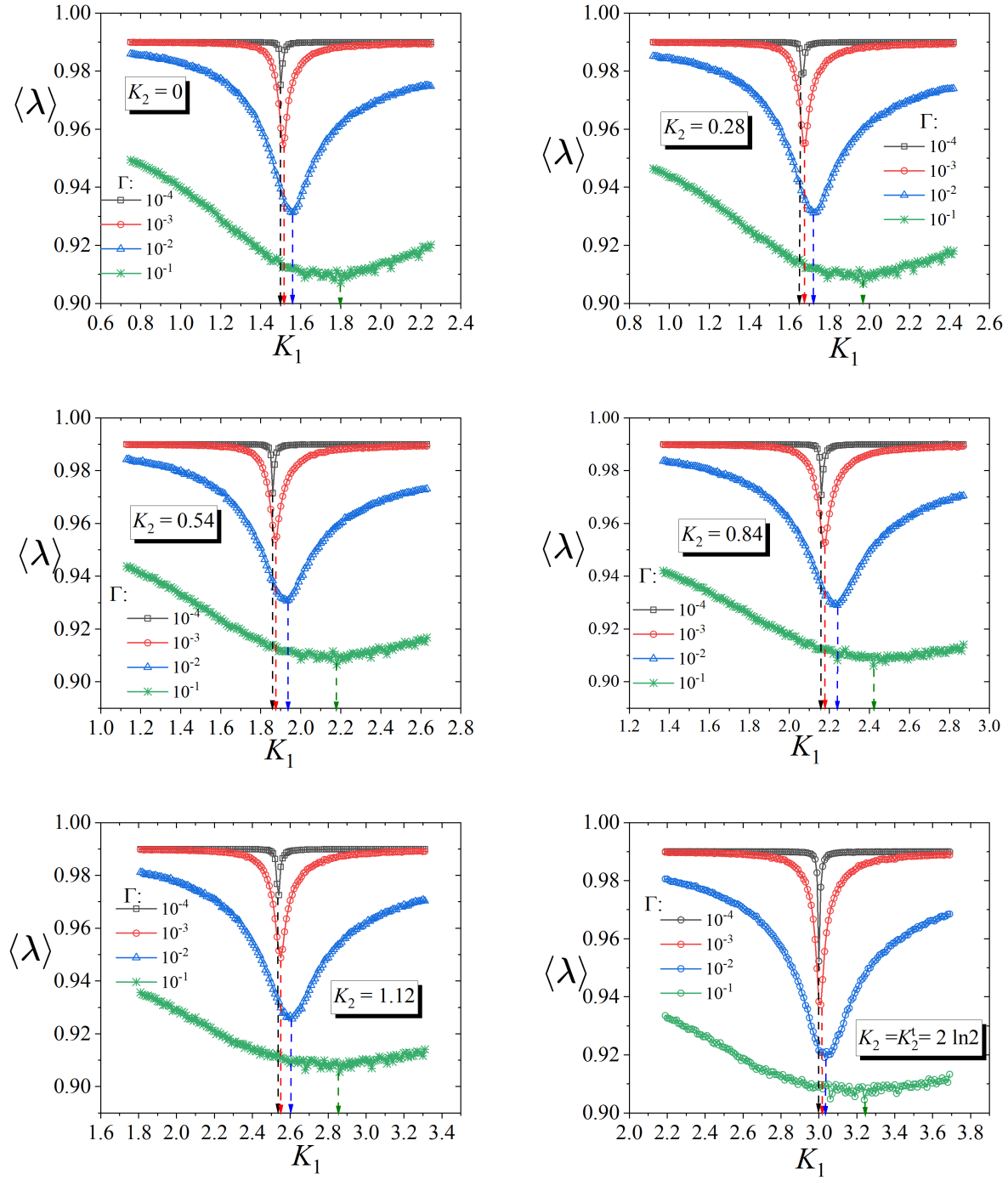


Figure 2. Average eigenvalue as a function of K_1 for different values of K_2 along the critical line.

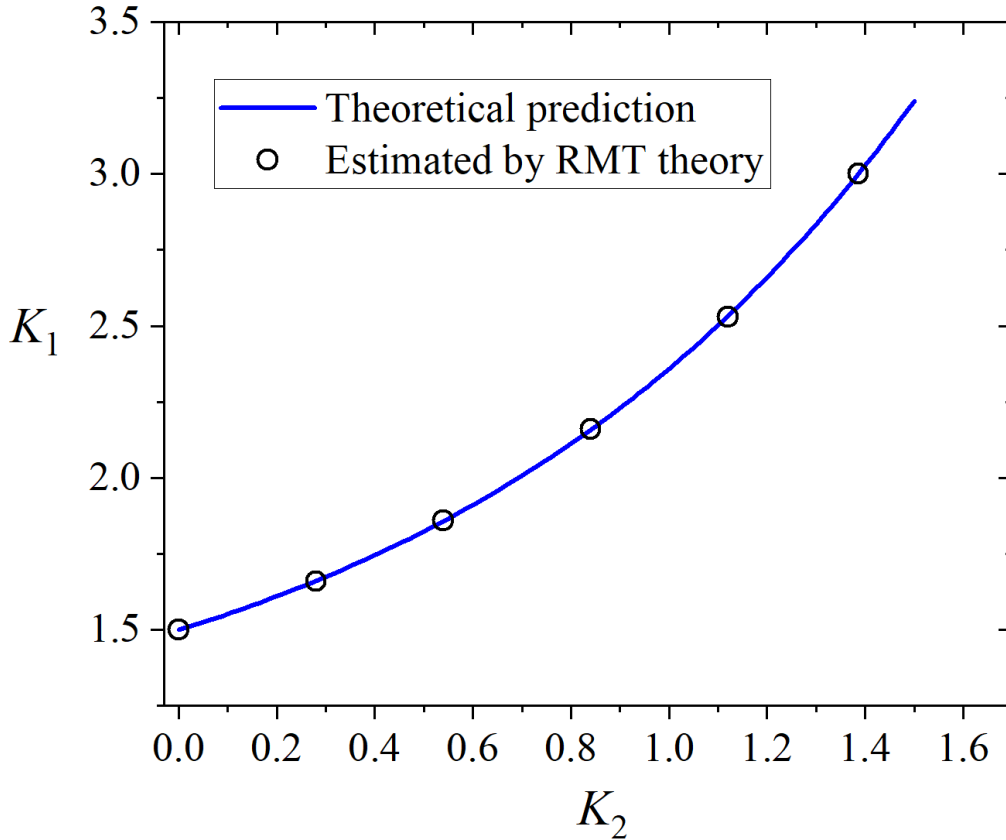


Figure 3. Critical values estimated using the RMT method for the Blume-Capel model align precisely with the theoretical curve.

This figure demonstrates that the RMT method accurately identifies the critical values. Notably, the use of Langevin equations to construct the matrices appears to mitigate the crossover effects observed in the simulations of the BC model (see [36]).

B. Characterization of the Chaotic Behavior in the Kicked Harper Model

Our algorithm constructs an ensemble of $N_{run} = 1000$ distinct matrices \mathcal{C} of dimension $N_{sample} \times N_{sample}$. These matrices correspond to N_{run} different initial conditions, which are randomly selected with $q_0, p_0 \in [0, 2\pi]$. We then diagonalize these matrices and organize the eigenvalues within the range $\lambda_{\min}^{(\text{Numerical})}$ to $\lambda_{\max}^{(\text{Numerical})}$. Using a fixed number of bins, $N_{bin} = 100$, we generate histograms to calculate $\rho(\lambda_i)$ in the same manner as we performed

for the Ising and BC model.

Thus, we obtain the average eigenvalue $\langle \lambda \rangle$ for each pair of values (K, L) as shown in Eq. 14. The results are presented in the first two diagrams: one considering the evolution of q and the other the evolution of p . Additionally, a third diagram combines the information from the previous two diagrams, denoted as $p - q$. Fig. 4 summarizes this information in a heat map.

The first diagram shows the results for the eigenvalues using the evolution of p , and the second diagram uses q . The third diagram considers the upper part ($L > K$) with values of p and the lower part ($L < K$).

In this diagram, we observe a large dark blue region, which corresponds to the area with a higher average value that we associate with chaos. Other regions are painted in different colors, indicating various structures that can be examined. In Fig. 4, we selected nine points in different regions to observe the $p \times q$ maps corresponding to each of these points. We begin with point 1 ($K = L = 1$). This point lies in a green region where yellow and green hues blend together. The corresponding phase space for this point can be observed in Fig. 5.

A stable structure emerges from this parameter choice. Investigating a nearby point ($K = 1.3$ and $L = 2$) we also observe a stable structure with small chaotic regions. This indefiniteness persists across different points studied, as illustrated in this plot. Stable islands can be observed in the "chaotic sea" for points indexed by 3 ($K = 2.6$ and $L = 2.6$) and 4 ($K = 3.425$ and $L = 3.425$) in the diagram, which are located in regions of low average values (ranging from yellow to black).

We will now investigate some symmetrical points. Let us focus on points 5 ($K = 3.3$ and $L = 9.625$) and 6 ($K = 9.625$ and $L = 3.3$). It is interesting to observe that both points exhibit patterns of holes in chaotic regions, but unlike points 3 and 4, these holes do not have well-defined boundaries. Additionally, the longitudinal direction of the holes is orthogonal when swapping K and L .

Next, we investigate another pair of symmetrical points: 7 ($K = 0.26$ and $L = 6.23$) and 8 ($K = 6.23$ and $L = 0.26$). In these points, we observe "insets" of stability within the chaotic regions. Finally, point 9 ($K = 8.67$ and $L = 9.5$) is located in the dark blue sea (chaotic region) 4. The phase space in Fig. 5 accurately describes this situation.

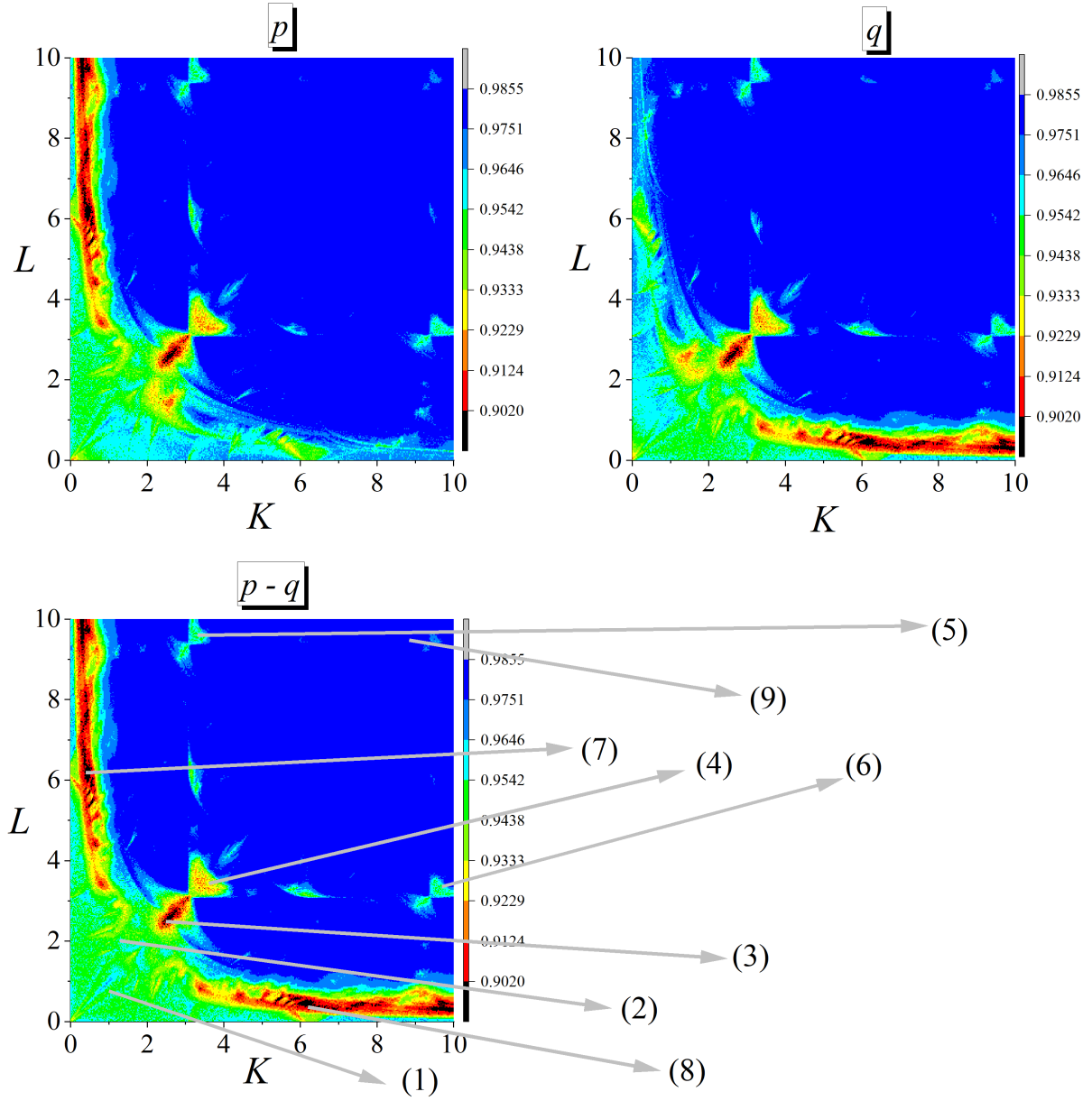


Figure 4. Average eigenvalue is attributed for each (K, L) parameter pair. The first diagram shows the results for the eigenvalues using the evolution of p , while the second uses q . A third diagram considers the upper part ($L > K$) with values of p , while a the lower part considers the values where ($L < K$). The arrows indicated in the plot highlight specific points for our analysis.

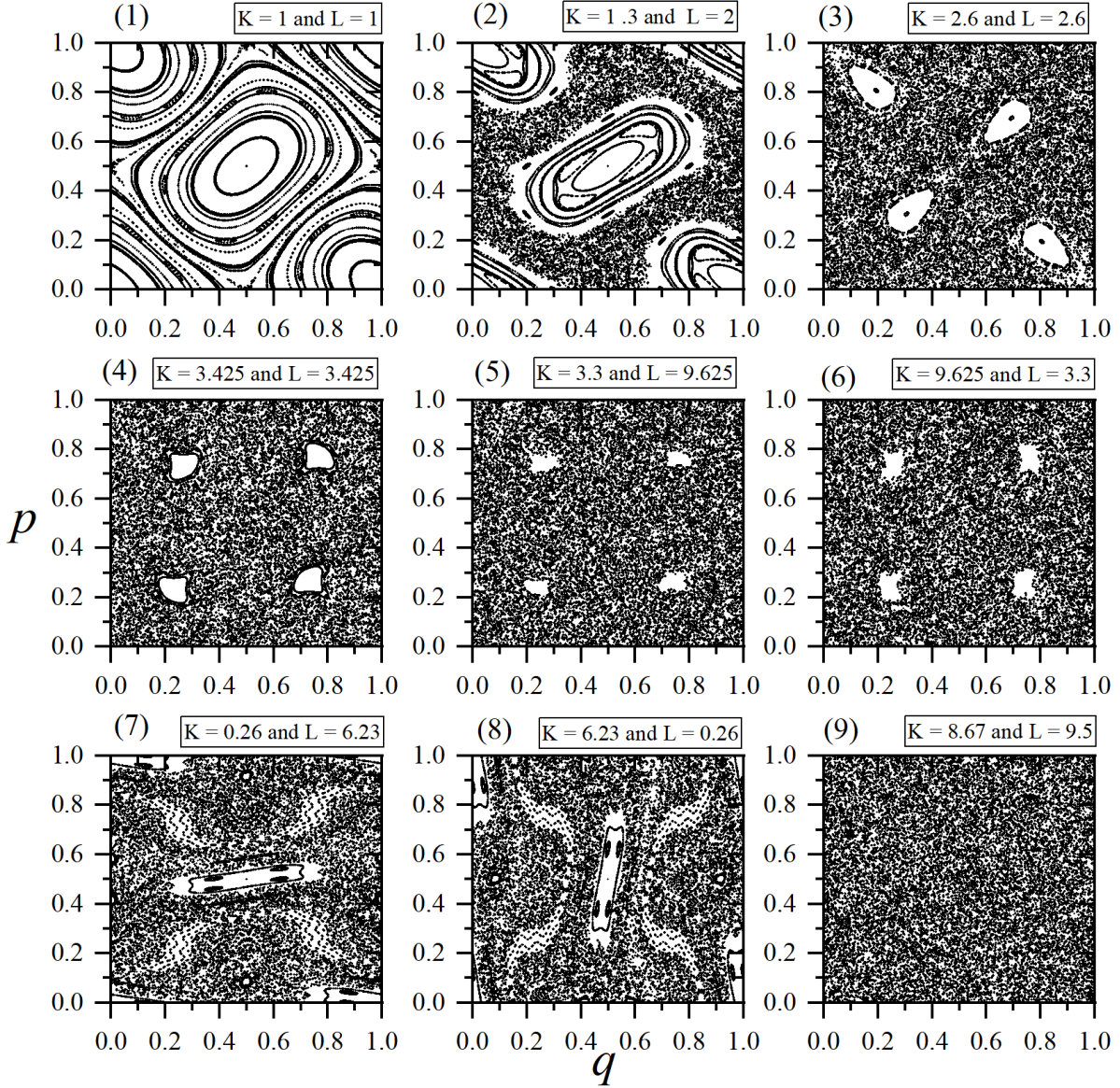


Figure 5. Maps $p \times q$ are obtained from specific points selected in the heat map shown in Fig. 4.

IV. CONCLUSIONS

We demonstrate that a flexible Random Matrices Theory method, based on Cross-correlation matrices, is highly effective for identifying phase transitions in maps from spin systems evolved by the Langevin equation. Similarly, the method is also very useful for describing chaotic behavior in deterministic maps with two parameters. In the first case,

the extremal values of the average eigenvalue of such matrices indicate criticality, while in the second case, smaller values of this parameter seem to indicate some degree of stability. The method captures the nuances and patterns of the systems at the differential equation level, thus avoiding the need for extensive numerical simulations, which warrants further investigation.

ACKNOWLEDGMENTS

R. da Silva extends gratitude to the Aguiá4 cluster at HPC-USP and the Lovelace cluster at IF-UFRGS for providing the computational resources. Additionally, thanks are due to CNPq for partial financial support of this work under grant 304575/2022-4. The authors would like to thank F. L. Metz for highlighting an important point regarding the Langevin equation.

-
- [1] M. L. Mehta, *Random Matrices*, Academic Press, Boston (1991)
 - [2] O. Bohigas, M. J. Giannoni, C. Schmit, *Phys. Rev. Lett.* **52**, 1 (1984)
 - [3] F. Haake, *Quantum Signatures of Chaos*, Springer-Verlag (2001)
 - [4] E. P. Wigner, On the Distribution of the Roots of Certain Symmetric Matrices, *Ann. Math.* **67**, 325 (1958)
 - [5] F. J. Dyson, *J. Math. Phys.* **3**, 140 (1962)
 - [6] V. Plerou, P. Gopikrishnan, B. Rosenow, L. N. Amaral, H. E. Stanley, *Phys. Rev. Lett.* **83**, 1471–1474 (1999)
 - [7] V. Plerou, P. Gopikrishnan, B. Rosenow, L. N. Amaral, H. E. Stanley, *Physica A* **287**, 374–382 (2000)
 - [8] H.E. Stanley , P. Gopikrishnan, V. Plerou, L.A.N. Amaral, *Physica A* **287** 339–361 (2000)
 - [9] L. Laloux, P. Cizeau, M. Potters, J-P. Bouchaud, *Int. J. Theor. Appl. Finance* **3**, 391 (2000)
 - [10] J-P. Bouchaud, M. Potters, *Theory of Financial Risks. From Statistical Physics to Risk Management*, University Press, Cambridge (2000)
 - [11] R. Bansal, B. S. Peterson, *Magn. Reson. Imaging* **77**, 69 (2021)
 - [12] F. L. Metz, P. I. Castillo, *Phys. Rev. Lett.* **117**, 104101 (2016)

- [13] F. L. Metz, D. A. Stariolo, *Phys. Rev. E* **92**, 042153 (2015)
- [14] T. Tome, M. de Oliveira, *Stochastic Dynamics and Irreversibility*, Springer (2014)
- [15] N. G. Van Kampen, *Stochastic Process in Physics and Chemistry*, North-Holland (2007)
- [16] F. J. Dyson, *J. Math. Phys.* **3**, 1191 (1962)
- [17] A. J. Lichtenberg, M. A. Lieberman, *Regular and chaotic dynamics*, Springer (1992)
- [18] H. Goldstein, *Classical Mechanics*, Addison-Wesley, EUA (1951)
- [19] M. Henkel, M. Pleimling, *Non-equilibrium Phase Transitions, Vol. 2: Ageing and Dynamical Scaling far from Equilibrium*, Springer, Dordrecht (2010)
- [20] R. da Silva, *Int. J. Mod. Phys. C*, 2350061 (2023)
- [21] R. da Silva, E. Venites, S. D. Prado, J. R. Drugowich de Felicio, *Int. J. Mod. Phys. C*, 2450163 (2024)
- [22] R. da Silva, H. C. M. Fernandes, E. Venites Filho, Sandra D. Prado, J. R. Drugowich de Felicio, *Braz. J. Phys.* **53**, 80 (2023)
- [23] T. Vinayak, T. Prosen, B. Buca, T. H. Seligman, *EPL* **108**, 20006 (2014)
- [24] S. Biswas, F. Leyvraz, P.M. Castillero, T.H. Seligman, *Sci. Rep.* **7** 40506 (2017)
- [25] R. da Silva, S. D. Prado, *Dynamics* **3**, 777 (2023)
- [26] R. Artuso, F. Borgonovi, I. Guarneri, L. Rebuzzini, G. Casati *Phys. Rev. Lett.* **69**, 3302 (1992)
- [27] J. Wishart, The Generalised Product Moment Distribution in Samples from a Normal Multivariate Population, *Biometrika* **20A**, 32–52 (1928)
- [28] Vinayak, T. H. Seligman, Time series, correlation matrices and random matrix models, *AIP Conf. Proc.* **1575**, 196–217 (2014)
- [29] G. Livan, M. Novaes, P. Vivo, *Introduction to Random Matrices, Theory and Practice*, Springer (2018)
- [30] C. Recher, M. Kieburg, T. Guhr, Eigenvalue Densities of Real and Complex Wishart Correlation Matrices, *Phys. Rev. Lett.* **105**, 244101 (2010)
- [31] V. A. Marcenko, L. A. Pastur, *Math. USSR Sb.* **1** 457 (1967)
- [32] A.M. Sengupta, P. P. Mitra, *Phys. Rev. E* **60**, 3389 (1999)
- [33] R. da Silva. D. E. Peretti, S. D. Prado, *Appl. Math. Model.* **40**, 10689 (2016)
- [34] R. da Silva, S. D. Prado, H. A. Fernandes, *Commun. Nonlinear Sci. Numer. Simul.* **51**, 105 (2017)
- [35] Jason A. C. Gallas, *Phys. Rev. E* **48**, R4158 (1993)

[36] Eliseu V. Filho, R. da Silva, J. R. Drugowich de Felicio, *Entropy* **26**, 395 (2024)